Charge transport and localization in nanocrystalline CdS films: A time-resolved terahertz spectroscopy study

Z. Mics,[1] H. Němec,[1] I. Rychetský,[1] P. Kužel,[1,*] P. Formánek,[2] P. Malý,[3] and P. Němec[3]
[1]*Institute of Physics, Academy of Sciences of the Czech Republic, Prague, CZ-182 21, Czech Republic*
[2]*Institut für Strukturphysik, Technische Universität Dresden, D-01062 Dresden, Germany*
[3]*Faculty of Mathematics and Physics, Charles University in Prague, Prague, CZ-121 16, Czech Republic*
(Received 11 March 2011; published 28 April 2011)

Assessment of characteristic length and time scales of the charge localization in nanostructured semiconductors is a key point for understanding the initial stage of carrier transport after photoexcitation. A concerted use of time-resolved terahertz spectroscopy and Monte Carlo simulations of the motion of confined electrons allow us to obtain this information and develop a quantitative microscopic model of the electron transport in a nanocrystalline CdS film. A weak localization is observed inside individual nanocrystals while much stronger localization stems from the existence of nanocrystal clusters partially surrounded by voids. The efficiency of the short-range transport is controlled by the excess energy of electrons: Its increase enhances the conductive coupling between adjacent nanocrystals and clusters. Relaxation of electrons with high excess energy then leads to a decrease of their mobility on a subpicosecond time scale. Filling of conduction-band states by increasing the optical pump fluence allows us to maintain a high level of conductive coupling even at later times.

DOI: 10.1103/PhysRevB.83.155326 PACS number(s): 78.67.Bf, 72.20.−i, 73.23.−b, 78.47.D−

I. INTRODUCTION

Semiconductor nanocrystals (NCs) exhibit a plethora of new electronic and optical phenomena owing to their increased surface-to-volume ratio and carrier confinement.[1] However, the absence of a long-range crystal order fundamentally complicates the charge transport in NC films. The underlying physics is very complex as it involves a chain of processes occurring on several different space and time scales.[2] Understanding ultrafast photoconductivity mechanisms in nanostructured semiconductors is of crucial interest for basic and applied science since many applications such as solar cells inherently rely on efficient charge transport.[3] Transport properties on a nanoscale and at the earliest times after photoexcitation usually impose the intrinsic limit on the drift mobility;[4] however, their investigation is particularly challenging, namely, due to the lack of direct experimental methods.

A terahertz (THz) spectral region contains rich information about nanoscaled systems such as conductivity mechanisms, carrier confinement, and material morphology.[5,6] A quantitative interpretation of the conductivity spectra requires a microscopic theoretical framework[7] that is able to connect the measured macroscopic spectra with the local properties (charge transport within and among nanograins and local depolarization fields). A thorough application of this approach allows us to develop here the potential of time-resolved THz spectroscopy for studies of transport in nanoscaled materials.

We selected the NC films of CdS for this research because it is a well-established model material for investigating the fundamental physical behavior of confined electrons in nanoobjects. In particular, we wish to contribute to the discussion of the long-lasting controversy that NC films show quantum confinement of charges, which is clearly apparent in the optical absorption and emission spectra, and, simultaneously, a long-range bulklike transport in the electrical measurements.[8] The advantage of using THz spectroscopy for this research comes from the fact that it stays midway between the optical and electrical methods. The study was motivated not only by the fundamental research but also by potential applications in the field of optoelectronics and photovoltaics. The CdS nanocrystalline films prepared by chemical bath deposition (CBD) are used, for example, as buffer layers in highly efficient $Cu(In,Ga)(S,Se)_2$ solar cells.[9]

II. EXPERIMENTAL DETAILS

The reported results were obtained in the sample with a film thickness of 1.3 μm that was deposited at 90 °C on a fused silica substrate by ammonia-free CBD.[10] To make the preparation conditions similar to those used for the growth of the buffer layer of solar cells,[9] the as-prepared film was heat treated at 400 °C for 45 min, which resulted in a growth of NCs (Ref. 10) with a final average NC diameter of 10.4 nm. The prepared films are formed by closely spaced NCs, however, they are not homogeneous on the submicrometer scale, as was reported recently for CdSe nanocrystalline films.[11] The porosity of the CdS layer prepared by CBD is clearly apparent from the transmission electron microscopy (TEM) picture of the film cross section shown in Fig. 1. This morphology is quite typical for thin semiconducting films used for the preparation of solar cells.[9] We note that the sample used for TEM was prepared in a very similar way to the one used for the time-resolved study—the only significant difference is a smaller film thickness, which is favorable for TEM.

Here we employ an optical pump-THz probe technique as a contactless tool to characterize the transient conductivity on an ultrafast time scale.[12] We used a typical setup based on a femtosecond optical Ti:sapphire amplifier—details about our experiment are provided in Ref. 13. In the majority of experiments the optical excitation of the sample was achieved by the second harmonic with a mean wavelength of $\lambda_L =$ 400 nm and a pulse length of 100 fs. In additional control experiments the output of an optical parametric amplifier (TOPAS) at 510 nm was used. The variation of the NC

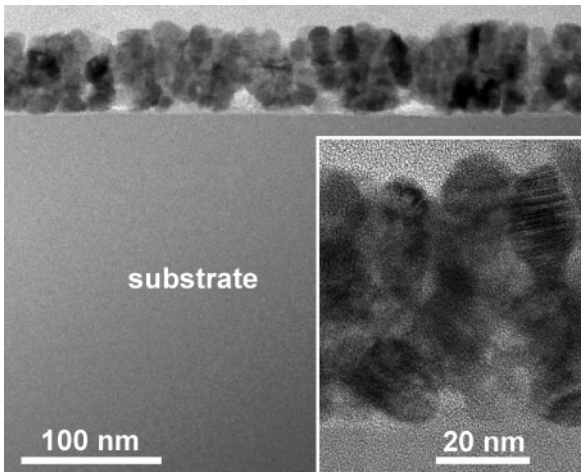

FIG. 1. TEM image of the cross section of a CdS film prepared by CBD.

response with the pump pulse fluence (i.e., with the initial concentration of conduction-band carriers) is a very important parameter which helps to assess the role of the depolarization fields[6] and the change of the nature of the transport due to conduction-band filling as described below. For this reason we carefully measured the incident pump fluence for each experimental run. Note that from this quantity we can easily determine the number of excitation events n_{exc} per laser pulse and per unit volume; however, the carrier density N is in principle unknown without knowledge of the quantum yield of the excitation process.

The photoconductivity of the sample was probed using delayed broadband single-cycle THz pulses in the range of 0.2–2 THz. We measured the time profile $E_0(t)$ of the THz pulse transmitted through the unexcited sample and its change induced by the photoexcitation $\Delta E(t,t_p)$; t_p is the pump-probe delay time.[13] From these data we calculated the transient conductivity spectra $\Delta\sigma(\omega,t_p)$ of the sample.[13] The transient conductivity normalized by the charge density $e \times N$ provides the carrier mobility, which is a single-carrier response function to a probing electric δ pulse. The experiments provide directly the product of the mobility $\mu(\omega,t_p)$ and the quantum yield $\xi(t_p) = N(t_p)/n_{\mathrm{exc}}$ of mobile charge carriers: $\mu\xi = \Delta\sigma/(n_{\mathrm{exc}}e)$.[6] Note that both the carrier density N and the mobility μ are generally time (t_p) dependent.

III. EXPERIMENTAL RESULTS AN DISCUSSION

The CdS NC films are strongly inhomogeneous systems; therefore, an applied electric field is screened by the depolarization field. The charge carriers in NCs respond to the local THz electric field, which may significantly differ from that of the applied THz probe. This means that the measured (macroscopic) effective conductivity may essentially differ from the intrinsic (microscopic) conductivity of carriers in the NCs. This can be described using an effective-medium approximation.[6,14] With our experimental technique we indirectly control the depolarization fields by varying the pump intensity: Our measured conductivities range from 5 to 550 $\Omega^{-1}\,\mathrm{cm}^{-1}$, which corresponds to a conductive contribution to the relative permittivity $\Delta\sigma/(\omega\varepsilon_0)$ in the range of 9–1000.

In CdS the effective mass of holes is at least three times larger than the effective mass of electrons[15] and the size of the NCs in the studied sample exceeds the excitonic Bohr radius [3 nm in CdS (Ref. 16)]. Consequently, the quantum confinement-induced changes of the band structure of the NCs are negligible[17] and the conductivity in NC CdS is dominated by bandlike motion of electrons with bulk effective mass, which can be described by the classical equations of motion. To account for the electron localization, which plays a crucial role in the microscopic conductivity of NC materials, we characterize the interaction of electrons with the NC boundaries in terms of probabilities of electron scattering and reflection following the method described in Ref. 7.

We discuss two kinds of experimental results. (i) Electron mobility spectra at selected pump-probe delays; comparison of such spectra with the results of simulations allows us to determine the nature of carrier transport and the degree of carrier localization in CdS NCs. (ii) THz kinetics representing the evolution of spectrally averaged THz photoconductivity versus pump-probe delay: They reflect the evolution of the carrier mobility (describing the possible change of the nature of carrier transport due to, e.g., carrier localization or energy relaxation) and the carrier population decay in the conduction band (due to trapping or recombination).

A. Spectral response of carriers

The measured conductivity spectra of NC CdS are displayed in Fig. 2(a). Their shape does not change substantially upon variation of the photoexcitation density over a broad range of values; we can then safely conclude that the NCs are dielectrically percolated and the effect of depolarization fields can be accounted for by a simple amplitude scaling of the whole spectra (cf. left-hand and right-hand scales in Fig. 2).[6] This conclusion is also supported by the fact that the observed mobility values are comparable to the ones of a bulk crystal (Fig. 2).

Figure 2(a) shows that the real part of the electron mobility increases with increasing frequency. This means that the NCs do confine the motion of electrons, i.e., it is more probable that electrons are reflected onto NC boundaries than that they pass into another NC.

A more detailed analysis of the measured mobility spectra and their comparison with the simulations provides further hints about the carrier confinement. It was shown previously that the ac mobility spectra of an electron inside a potential well with perfectly reflecting walls can be reasonably approximated by a Debye relaxation,[4,6,18]

$$\mu_{\mathrm{ac}}(\omega) = \mu_{\mathrm{int}} \frac{1}{1 - i\pi^2 \frac{\mu_{\mathrm{int}} k_B T}{L^2 \omega e_0}}, \tag{1}$$

where L is the size of the box, T is the temperature, k_B is the Boltzmann constant, and $\mu_{\mathrm{int}} \approx 140\ \mathrm{cm}^2\ \mathrm{V}^{-1}\ \mathrm{s}^{-1}$ is the mobility of the electron inside the box [i.e., the mobility in bulk CdS—see spectra in Fig. 1(a)]. The real part of this function is concave only for

$$\omega > \frac{\pi^2 k_B T \mu_{\mathrm{int}}}{\sqrt{3} L^2 e_0}, \tag{2}$$

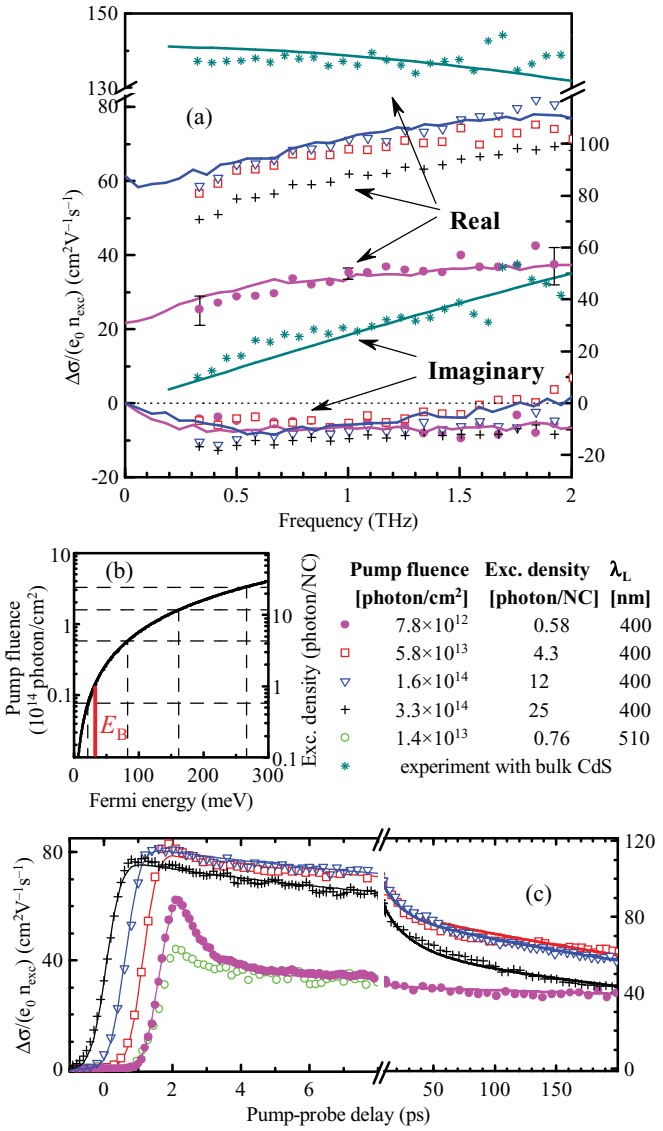

FIG. 2. (Color online) (a) Normalized transient conductivity spectra (yield-mobility product) measured 10 ps after photoexcitation; lines: simulations. (b) Pump fluence (and n_{exc}) vs photocarrier Fermi energy; zero energy corresponds to the bottom of the conduction band. The curve is calculated from the conduction-band density of states in CdS. Dashed lines indicate our experimental conditions; E_{B} is the barrier height stemming from the kinetic model. (c) THz kinetics (curves are horizontally shifted for clarity; the signal rise for each curve corresponds to the pump-probe overlap); lines: results of fits with the kinetic model. Left-hand scales: effective (macroscopic) conductivity. Right-hand scales: intrinsic (microscopic) conductivity.

and, comparing to our spectra which are concave above $\omega_{\mathrm{low}} \approx 2\pi \times 0.4$ THz, we deduce that

$$L \geqslant \sqrt{\frac{k_B T \mu_{\mathrm{int}} \pi^2}{\sqrt{3}\omega_{\mathrm{low}} e_0}} \approx 28 \text{ nm}. \tag{3}$$

In other words, it is not possible to explain the spectra by an electron confinement solely at the 10-nm scale corresponding to the NC size, but the electron motion must be at least partially blocked also on longer length scales. We attribute this phenomenon to electron localization in clusters of NCs. This picture of the CdS film morphology that is deduced from the measured charge carrier dynamics—i.e., an aggregation of individual NCs to clusters that are mutually separated—is in perfect agreement with the film morphology shown in Fig. 1.

The electron mobility was calculated using a Monte Carlo method described in Ref. 7. In modeling NC CdS we take into account the existence of the two length scales for the interaction of electrons with the boundaries: the size of NCs and the size of NC clusters. The larger scale has a variable size in our simulations and an independent set of parameters describing the electron scattering and reflection on the cluster boundary.

Our simulations show that the average size of the clusters is ∼40 nm and, upon interaction with the boundaries of a cluster, the probability of electron transport to another cluster is only 3% for the lowest photoexcitation fluences. In the same experimental conditions the probability of transition between NCs is much larger, ∼34%. Such a high value shows that the inter-NC transport is highly efficient, despite the quantum confinement of electrons in NCs. Upon increasing the photoexcitation fluence ($n_{\mathrm{exc}} \gtrsim 4.3$ photons/NC) the amplitude of the measured normalized conductivity (yield-mobility product) first abruptly increases: the probabilities of intercluster and interparticle transitions increase to $(10 \pm 2)\%$ and $(66 \pm 10)\%$, respectively; then they become approximately independent of the photon density. It means that at high pump fluences the NC boundaries practically do not confine the electron motion, and even the random momentum scattering on NC boundaries is partially suppressed. A small drop of the normalized conductivity amplitude at 3.3×10^{14} photons/cm^2 [Fig. 2(a)] is mostly related (by 60%) to the increased rate of carrier recombination with increasing carrier density [observed in Fig. 2(c)] and partly related to a decrease of the mobility due to carrier-carrier scattering in the volume on NCs at these high carrier densities.

In order to match the experimental data, the amplitude of all the simulated spectra was multiplied by a factor of 0.7. This factor, duly expressed as the ratio of the mobility-yield product obtained from the measured (effective) conductivity spectra and the microscopic mobility retrieved from the simulations, accounts for the depolarization fields and for the yield of the photoexcitation process. The value of 0.7 then corresponds to at most 20% of the voids within the Maxwell-Garnett approximation. The yield of the photoexcitation process must be then close to unity.

The enhanced conductive coupling between NCs observed with increasing excitation fluence can be explained by the presence of electrons with high excess energy. The initial excess energy of electrons with a 400-nm pump is ∼0.4 eV, and the electrons progressively relax to the bottom of the conduction band [Fig. 3(a)]. The conduction-band filling is observed at higher pump fluences, and consequently more electrons possess a sufficient excess energy even at later times to pass over the barriers at the NC boundaries [Fig. 3(c)]. All these findings deduced from the measured electron dynamics suggest a microscopic picture which is consistent with the film morphology. Individual NCs are closely packed together within clusters, and the interparticle transport of electrons is hindered by potential barriers at NC boundaries; these become

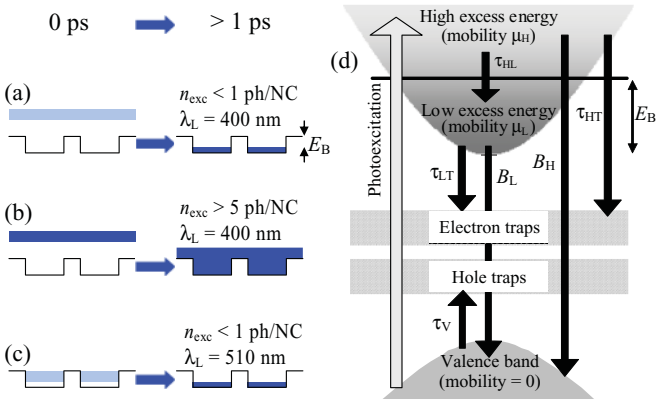

FIG. 3. (Color online) (a), (b), (c) Schemes illustrating the occupancy of the conduction-band states after photoexcitation (0 ps) and after the subsequent energy relaxation process (>1 ps) for various experimental conditions. (d) Scheme of the kinetic model. The symbols denoting the possible processes are described in the text.

highly permeable (66%) in a strongly excited sample. In contrast, larger pores can be found among the clusters and the much lower permeability of the cluster surface (10%) is then related to geometrical aspects: The intercluster transport may be possible only through channels between the pores where the clusters are in contact.

From the transient THz spectra we thus learn two important facts: (i) That the motion of electrons is influenced by the existence of two characteristic length scales and (ii) that the conduction-band electrons can be either in a high- or in a low-mobility state following their excess energy.

B. THz kinetic measurements

Our view receives strong support from the measurements of THz kinetics [Fig. 2(c)]. The normalized conductivity (yield-mobility product) raises immediately after photoexcitation to a value almost independent of the photoexcitation density. The subsequent dynamics consists of two parts: an ultrafast decay within ~1 ps after photoexcitation and a slow one occurring over the whole measured time window. In this paper we focus our analysis on the first part, which essentially provides information about the transport mechanisms. The second part is mainly related to the recombination of carriers. Here we provide only a qualitative interpretation of the observed behavior; longer pump-probe scans would be necessary in order to provide an unambiguous quantitative assessment of the recombination mechanisms.

The amplitude of the fast decay component is decreasing with increasing excitation density [see Fig. 2(c)]; below 8×10^{12} photons/cm^2 (the lowest fluence in our compilation of the measured data) it remains constant. The time constant of the slow component decay is found to be much longer than 200 ps at 8×10^{12} photons/cm^2 and it is decreasing with increasing fluence (~200 ps at 3.3×10^{14} photons/cm^2).

We explain the ultrafast decay of the electron mobility by an energy relaxation of electrons. At 400-nm excitation wavelength the electrons initially occupy energy levels above the barriers at the NC boundaries, and they are delocalized over the whole cluster; their mobility is high and essentially independent of their concentration. Due to the interaction with optical phonons the electrons relax to the bottom of the conduction band, where they become localized to a larger extent.

To describe quantitatively the energy relaxation of the electrons, we use a simple kinetic model with two levels [Fig. 3(d)]. The upper level represents electron states in the conduction band with high excess energy (delocalized over a cluster, mobility μ_H), the lower one represents electrons confined within the NCs (mobility μ_L). The energy relaxation of carriers corresponds to a transition from the upper to the lower state and it is accounted for by a decay of the upper level population with a time constant τ_{HL}; the density of available states in the lower level is limited due to the finite energy barrier height E_B, i.e., the transition rate from the μ_H states to the μ_L states slows down as the bottom of the conduction band becomes filled. In addition, the electrons can be trapped or they can undergo another kind of recombination with holes in the valence band.

From a simultaneous fit of all measured kinetics, we can reliably determine the parameters which characterize the carrier transport and which are essentially determined by the initial part of the kinetics ($\lesssim$20 ps): $\tau_{HL} = 0.54$ ps, $\mu_H = 96$ cm^2 V^{-1} s^{-1}, $\mu_L = 33$ cm^2 V^{-1} s^{-1}, and the density of low-excess-energy states is $N_L = 2.4 \times 10^{18}$ cm^{-3}, which corresponds to the barrier height $E_B = 33$ meV [cf. Fig. 3(b)]. Note that the values of the mobilities μ_H and μ_L were obtained from the fits of the kinetics shown in Fig. 2(c); these kinetics display an average electron mobility in the THz range without the spectral resolution. Comparing back with Fig. 2(a) we observe that the value of μ_L corresponds to the average value of the magenta (filled circles) curve in Fig. 2(a) ($n_{exc} = 0.58$ photons/NC) and that curves with higher excitation densities must be determined by a mix of the values of μ_H and μ_L.

While fitting the measured THz kinetics, we assumed that the recombination may be predominantly either due to a bimolecular electron-hole recombination process or by Auger recombination.

Auger recombination is a process which is expected to be enhanced in NCs due to the spatial confinement of charge carriers.[19] In this process one electron-hole pair recombines nonradiatively, giving its energy to another carrier, e.g., to an electron (*eeh* process) which is promoted to a state with a high excess energy in the conduction band (such states possess a higher mobility in our sample than those at the bottom of the conduction band). This in turn can lead to an enhancement of the conductivity in spite of the fact that the total number of excited carriers decreases. The localized carriers can also take part in the Auger process due to its Coulomb-interaction origin. However, taking into account the fact that the fast energy relaxation from the high-mobility to the low-mobility states in the conduction band is likely to be much faster than the Auger recombination process, a possible increase in the average mobility dynamics should be negligible.

In our fits we found that a dominant Auger recombination is not compatible with the shape of our kinetics in CdS, while a significant bimolecular recombination may take place: $B_H \approx 5 \times 10^{-22}$ cm^3 ps^{-1} and $B_L \approx 5 \times 10^{-21}$ cm^3 ps^{-1}. These values are similar to those found in 5-nm CdS NCs by Juodkazis *et al.*[20] These authors also reported the value of Auger recombination coefficient ~3×10^{-42} cm^6 ps^{-1}

which leads to the Auger recombination time of ∼130 ps for the highest excitation density we used in our experiments. However, our measurements were done in a limited time window and using a narrow range of excitation fluences; consequently, the Auger recombination could not be clearly distinguished from the bimolecular one in our data. On the one hand, this limits the accuracy of our determination of B_L and B_H, and, on the other hand, we can conclude that $\sim 3 \times 10^{-42}$ cm^6 ps^{-1} is the upper limit for the Auger coefficient in the CdS NCs grown by CBD.

To confirm our model of electron energy relaxation, we carried out additional experiments with photoexcitation at 510 nm. With a longer excitation wavelength the initial excess energy of electrons is lower and the upper state is initially much less populated [Fig. 3(c)]. Consequently, the relative amplitude of the decrease of electron mobility due to energy relaxation is expected to be smaller, which was indeed observed experimentally [see Fig. 2(c)].

C. Energy barriers

Although the energy barrier E_B determined above is close to the optical phonon frequency in CdS, it is unlikely that the energy barrier is related to lattice vibrations. In such a case, one expects a strong temperature dependence of the THz kinetics (pump-probe scans); however, we did not observe any significant changes in these kinetics down to lattice temperatures of at least 20 K (data not shown here).

We believe that the observed energy barrier E_B is related to an electrostatic interaction between an electron and a hole in the nanoparticle. Indeed, it is known that the holes become rapidly trapped mostly within the NC where they were created.[21] The energy required to move an electron from the NC surface to infinity in an unscreened Coulomb potential of a hole in the center of the NC,

$$U = \frac{1}{4\pi\varepsilon_0\varepsilon}\frac{e^2}{r_{NC}}, \tag{4}$$

is ∼30 meV (here $\varepsilon \approx 9$ is the permittivity of CdS and $r_{NC} \approx 5$ nm is the NC radius).

These energy barriers are too low to cause by themselves the electron quantum confinement observed by optical methods; we propose the following picture. The NCs are separated by potential barriers, which do confine electrons, but at the same time they are sufficiently narrow to permit electron tunneling. The Coulombic electrostatic potential of a hole lowers the potential inside the NC in which the hole resides. The energetic barrier reported here then represents the energy difference between the NCs while the presence of the confining potential is at the origin of a limited permeability of the NCs surface for electron transport. Interestingly, the carrier concentration of $n_{exc} \approx 1$ corresponds approximately to the state where the conduction band is filled up to E_B. For densities exceeding a few excitations per nanoparticle, besides the effect of the band filling, the permeability of the NCs may be enhanced because the Coulombic barriers may cease to exist.

In order to receive further confirmation of our hypothesis on the Coulombic origin of the energy barriers, we currently carry out experiments with variable sizes of NCs and at several temperatures. The importance of the dynamically (i.e., by photoexcitation) induced Coulomb interaction in the ultrafast carrier transport has been demonstrated, e.g., in dye-sensitized ZnO nanoparticles, where the presence of the dye cation leads to a dramatic reduction in the electron mobility.[5] Also, attachment of cyanide anions to a CdS NC surface caused a static band-edge shift, indicating an increase of the electron localization.[22]

The behavior of charge mobility in the NC films resembles that found in conducting polymer films. The conduction mechanism is, however, different: The conduction-band electrons in NC films occasionally hit energetic barriers, whereas transport in polymer films is typically viewed as charge hopping among localized states with a Gaussian distribution of energy. In a low-band-gap polyphenylene copolymer and a fullerene blend[18] it was found that the initial hole mobility rapidly decreases by at least an order of magnitude within less than 1 ps: The holes lose their excess energy and the jumps over the barriers become less probable. In this system two length scales of the carrier confinement have also been observed in the THz spectra: One localization mechanism is introduced by the ends of the polymer chains and the other by the potential barriers inside the chains. Chemical doping of the polymers raises the quasi-Fermi level, which leads to a decrease of the activation energy and an increase in the charge mobility.[23] Analogically, sufficient n doping of the CdS NCs may shift the Fermi level above the band gap, and we expect that this would prevent the mobility reduction at later times and thus significantly improve the drift mobility in the film. This could lead to a new perspective for the preparation of highly porous materials with improved charge mobility.

IV. CONCLUSION

To conclude, we observed and identified mechanisms which strongly influence the charge mobility on the ultrafast time scale in CdS NCs: transport over two nanoscopic length scales, energy relaxation, and Coulombic interaction. These phenomena seem to be a more general effect encountered in nanostructured and/or disordered photoexcited semiconductor systems. The experiments clearly indicate that the nanoscopic transport in CdS NCs involves the length scale of individual NCs (∼10 nm), where the interparticle transport is controlled by ∼30 meV Coulombic energy barriers, and the length scale of the NC clusters (∼40 nm), where the transport is strongly influenced by the presence of air voids between clusters. We also demonstrate the coexistence of quantum confinement of electrons and their efficient inter-NC transport. The ultrafast photoconductivity is governed by the relaxation of the electron energy and by filling the states in the conduction band. In this sense, varying the excitation density allows one to tune the conductive coupling of NCs.

ACKNOWLEDGMENTS

Financial support by the Czech Science Foundation (projects 202/09/H0041, 202/09/0430 and 202/09/P099), Academy of Sciences of the Czech Republic (projects A100100902 and AVOZ10100520), and Ministry of Education of the Czech Republic (project LC-512 and the research plan MSM0021620834) is acknowledged.

*kuzelp@fzu.cz

[1] A. Rogach, *Semiconductor Nanocrystal Quantum Dots* (Springer, Berlin, 2008).
[2] J. Nelson, J. J. Kwiatkowski, J. Kirkpatrick, and J. M. Frost, Acc. Chem. Res. **42**, 1768 (2009).
[3] M. Grätzel, J. Photochem. Photobiol., A **164**, 3 (2004).
[4] P. Prins, F. C. Grozema, J. M. Schins, S. Patil, U. Scherf, and L. D. A. Siebbeles, Phys. Rev. Lett. **96**, 146601 (2006).
[5] H. Němec, J. Rochford, O. Taratula, E. Galoppini, P. Kužel, T. Polívka, A. Yartsev, and V. Sundström, Phys. Rev. Lett. **104**, 197401 (2010).
[6] H. Němec, P. Kužel, and V. Sundström, J. Photochem. Photobiol., A **215**, 123 (2010).
[7] H. Němec, P. Kužel, and V. Sundström, Phys. Rev. B **79**, 115309 (2009).
[8] G. Hodes, A. Albu-Yaron, F. Decker, and P. Motisuke, Phys. Rev. B **36**, 4215 (1987).
[9] S. Taunier, J. Sicx-Kurdi, P. P. Grand, A. Chomont, O. Ramdani, L. Parissi, P. Panheleux, N. Naghavi, C. Hubert, M. Ben-Farah, J. P. Fauvarque, J. Connolly, O. Roussel, P. Mogensen, E. Mahe, J. F. Guillemoles, D. Lincot, and O. Kerrec, Thin Solid Films **480-481**, 526 (2005).
[10] P. Němec, I. Němec, P. Nahálková, K. Knížek, and P. Malý, J. Cryst. Growth **240**, 484 (2002).
[11] M. Šimurda, P. Němec, P. Formánek, I. Němec, Y. Němcová, and P. Malý, Thin Solid Films **511**, 71 (2006).
[12] F. A. Hegmann, O. Ostroverkhova, and D. G. Cooke, in *Photophysics of Molecular Materials*, edited by G. Lanzani (Wiley, Weinheim, 2006), pp. 367–428.
[13] L. Fekete, P. Kužel, H. Němec, F. Kadlec, A. Dejneka, J. Stuchlík, and A. Fejfar, Phys. Rev. B **79**, 115306 (2009).
[14] E. Hendry, M. Koeberg, B. O'Regan, and M. Bonn, Nano Lett. **6**, 755 (2006).
[15] P. P. Horley, V. V. Gorley, P. M. Gorley, J. Gonzalez-Hernandez, and Y. V. Vorobiev, Thin Solid Films **480-481**, 373 (2005).
[16] M. V. Rama Krishna and R. A. Friesner, J. Chem. Phys. **95**, 8309 (1991).
[17] P. Horodyská, P. Němec, D. Sprinzl, P. Malý, V. N. Gladilin, and J. T. Devreese, Phys. Rev. B **81**, 045301 (2010).
[18] H. Němec, H. K. Nienhuys, E. Perzon, F. Zhang, O. Inganäs, P. Kužel, and V. Sundström, Phys. Rev. B **79**, 245326 (2009).
[19] I. Robel, R. Gresback, U. Kortshagen, R. D. Schaller, and V. I. Klimov, Phys. Rev. Lett. **102**, 177404 (2009).
[20] S. Juodkazis, E. Bernstein, and J. C. Plenet, Opt. Commun. **148**, 242 (1998).
[21] V. I. Klimov, Ch. J. Schwarz, D. W. McBranch, C. A. Leatherdale, and M. G. Bawendi, Phys. Rev. B **60**, R2177 (1999).
[22] S. K. Sarkar, N. Chandrasekharan, S. Gorer, and G. Hodes, Appl. Phys. Lett. **81**, 5045 (2002).
[23] F. Laquai, G. Wegner, and H. Bässler, Philos. Trans. R. Soc. London A **365**, 1473 (2007).